Polym. Bull. (2012) 69:81–94
DOI 10.1007/s00289-012-0727-9

ORIGINAL PAPER

Characterization and electrochemical behaviors of honeycomb-patterned poly(*N*-vinylcarbazole)/polystyrene composite films

Phung Xuan Thinh · C. Basavaraja · D. G. Kim · Do Sung Huh

Received: 3 January 2012 / Revised: 24 February 2012 / Accepted: 24 February 2012 /
Published online: 4 March 2012

Abstract Poly(*N*-vinylcarbazole)/polystyrene composites were prepared through simple radical polymerization of *N*-vinylcarbazole in the presence of polystyrene. Honeycomb-patterned composite thin films were fabricated by casting the composite solutions under humid conditions. The scanning electron microscopy (SEM) images of the resulting honeycomb pattern on the composites show a higher regular structure compared to those of films prepared from the poly(*N*-vinylcarbazole) homopolymer. The pressure-area isotherms and photoelectrochemical behaviors of the patterned films were also observed. The photoconductivity of the patterned thin films increased with increasing poly(*N*-vinylcarbazole) concentration. This enhancement is attributed to the effects of the honeycomb structures and the charge transfer across the donor/acceptor hybrid interface in the composite films.

Keywords Poly(*N*-vinylcarbazole) · Polystyrene · Honeycomb-patterned film · Photoconductivity · Polymer composite

Introduction

Honeycomb-patterned thin films have attracted considerable attention because of their potential use in micro-reactors [1], separation processes [2], electronics, photonics [3, 4], and biotechnology [5, 6]. One of the many methods for fabricating porous polymer films [7–10] is the breath-figure formation, which is a simple and useful technique [11, 12]. Through this method, porous films from many kinds of substrates, including star polymers, block copolymers, proteins, and polymer composites, have been fabricated under humid conditions [13, 14].

P. X. Thinh · C. Basavaraja · D. G. Kim · D. S. Huh (✉)
Department of Chemistry and Institute of Basic Science, Inje University, Kimhae, Kyungnam 621-749, South Korea
e-mail: chemhds@inje.ac.kr

In recent years, conducting polymeric materials have attracted considerable attention because of their optical and electrical properties as well as applications in many fields. Among the different conducting polymeric materials currently available, poly(*N*-vinylcarbazole) (PVK) has emerged as one of the more useful materials for electro-optically active applications, such as in light-emitting diodes and xerography [15, 16]. Moreover, PVK is considered an ideal model of a nonconjugated photoconducting polymer with strong electron-donor properties. Reactions with vinylcarbazole can easily be performed in bulk, solutions, suspensions, or precipitations. Vinylcarbazole can stabilize electron-deficient centers through resonance with the nonbonding electron pair of the nitrogen atom of its carbazole ring, making this compound a popular polymerization material [16, 17].

Porous thin film fabrication from conducting polymers such as PVK can be useful in many areas of nanoscience and technology, including nanoelectronics, nanodevices, catalysts, sensors, and others. Heng et al. [18] demonstrated that the porous structure of photoelectrically functional polymer films can significantly improve the photocurrent generation compared with those of the corresponding smooth films. However, the poor mechanical properties of PVK, particularly its brittleness, and difficult processing, have become major obstacles in the fabrication of porous thin films from pure PVK. A proper selection of functionalized dopants can improve the features of PVK polymer composites. The dopants can convert this material into better polymers that possess excellent mechanical, optical, and electrical properties.

Polystyrene (PS) is an important material with good mechanical properties, including high-impact strength, good heat resistance, good thermal and oxidative stabilities, and remarkable optical property with a high-refractive index. Given its hydrophobicity, PS is also very suitable for the fabrication of highly ordered films through the breath-figure method. The combination of PVK and PS in one material could improve the processability of the resulting PVK composite. Thus, the stable honeycomb-patterned PVK composite films can be easily fabricated.

In this study, a new type of PVK–PS composite was synthesized through free radical polymerization of *N*-vinylcarbazole (NVC) in the presence of PS. The obtained PVK–PS polymer composites were characterized via Fourier-transform infrared (FTIR) spectrometry and ultraviolet–visible (UV–Vis) spectroscopy, and the thermal behavior was determined via thermogravimetric analysis (TGA) and differential scanning calorimetry (DSC). The morphology of the honeycomb-patterned thin films, fabricated by casting the composite solution under humid conditions, was determined using scanning electron microscopy (SEM). The pressure-area isotherms and photoconductivity of the honeycomb-patterned films were obtained.

Experimental details

Materials

NVC (98%, Aldrich) was purified via recrystallization using absolute methanol and dried in vacuum at 30 °C. Styrene (99.5%, Aldrich) was separated from the initiator

by washing twice with 5% aqueous sodium bisulfate, twice with 8% aqueous sodium hydroxide, and finally with distilled water until the solution pH was 7. The monomer was dried over anhydrous magnesium sulfate and distilled under reduced pressure before use [19]. Azobisisobutyronitrile (AIBN, 99%), benzoyl peroxide (BPO, 98%), sodium hydroxide (98%), sodium sulfate (65%), methanol (≥99.8%), and chloroform (≥99%) were used as-received from Aldrich without further purification. Deionized (DI) water was used in all experiments.

Synthesis of polystyrene

Purified and dried styrene (10 g) was dissolved in 30 mL toluene. BPO (150 mg) was added to the styrene solution at room temperature, and the mixture was swirled until BPO was dissolved. The oxygen was then removed, and the mixture was heated in an oil bath at 80 °C for 24 h under a nitrogen atmosphere. The mixture was then removed from the oil bath and allowed to cool to ambient conditions. White precipitate was formed after the addition of an excess amount of methanol. The precipitate was collected, washed several times with distilled methanol and water, and dried at 60 °C in a vacuum oven for approximately 24 h [20]. The average molecular weight (M_w) of PS was determined using gel permeation chromatography; the average molecular weight is 42,500 (PDI = 1.52).

Synthesis of PVK and the PVK–PS polymer composites

Different concentrations (in wt%) of the NVC monomer were initially dissolved in 15 mL toluene containing 5 g PS in a three-necked round-bottom flask. The mixtures were sonicated for 1 h at room temperature. AIBN (1.5 wt% of NVC monomer) was then added to the solution as an initiator. After degasification under vacuum, polymerization was performed in an oil bath at 70 °C for 24 h under nitrogen atmosphere [21]. The flask was then removed from the oil bath and allowed to cool to ambient temperature. The reaction mixtures were precipitated using an excess amount of methanol. The white precipitate was collected, washed several times with distilled methanol and water, and dried in a vacuum. The initial amount of NVC used for the preparation of the composites varied by 15, 30, and 50 wt% of the constant amount of PS, and the corresponding polymer composites formed through the composition were labeled as PVK-15, PVK-30, and PVK-50, respectively.

A process similar to that described above was performed for the synthesis of the PVK homopolymer, but without the addition of the PS polymer.

The concentration of PVK in the PVK–PS composites was approximately determined by measuring the weight of the reaction products. The actual percentage of PVK in PVK-15, PVK-30, and PVK-50 composites is 11.5%, 20.5%, and 32%, respectively.

The IR spectra of the composite samples pelletized with potassium bromide (KBr) were obtained using an FTIR spectrophotometer (Model 1600, Perkin-Elmer). Approximately 60 scans were signal-averaged at a resolution of 2 cm^{-1} from 4,000 to 400 cm^{-1}. The UV–Vis spectra of the composites were also obtained

using a Shimadzu UV–Vis-near IR (NIR) spectrophotometer (UV-3101PC). The thermal properties were determined through TGA (Perkin-Elmer TGA 7) at 25–300 °C, and DSC (Perkin-Elmer DSC 7) at 25–800 °C and a heating rate of 10 °C/min under a nitrogen atmosphere.

Fabrication of the honeycomb-patterned thin films from the PVK–PS polymer composites

A solution containing 0.25 g of the PVK–PS composites and 4 mL chloroform was stirred at room temperature for about 1 h and then cast on a glass Petri dish at 25 °C under a relative humidity of 60%. The porous film was formed through the condensation and deposition of water droplets on the solution surface by evaporative cooling [22]. The morphology of the obtained film was determined through scanning electron microscopy (SEM, COXEM CX-100). To determine the surface pressure-area isotherm behavior, the film was exposed to a surface pressure of 25 mN m^{-1}, with a barrier speed of 2.5 mm s^{-1}. Photocurrent measurements were performed using a PAR model 5206 lock-in amplifier. A 150 W white light source was illuminated at a distance of 5–10 cm from the working electrode to determine the photoelectrochemical current response. A 10^{-2} mol dm^{-3} solution of $LiClO_4$ was used to measure the photocurrent in the electrodes at 0.4 V.

Results and discussion

Spectral characterization of PS, PVK, and PVK–PS composites

Figure 1 shows the FTIR spectra and Table 1 summarizes the major FTIR peaks of the synthesized PS, PVK, PVK-30, and PVK-50, along with their probable assignments. The spectra of PS at the 2,800–3,100 cm^{-1} frequency range are attributed to C–H stretching vibrations in the main chain and in the aromatic rings, and the peaks at 1601, 1493, 1028, 756, and 698 cm^{-1} are attributed to the deformation and skeletal vibrations of C–H in the compound [23]. The PVK spectra show bands at the 700–800 cm^{-1} range (out-of-plane deformation and stretching vibration of aromatic –C–H), 1,100–1,150 cm^{-1} (in-plane deformation and stretching vibration of aromatic –C–H), and 1,600 cm^{-1} (C=C stretching). The presence of the PS polymer in the composite and the changes in its concentration (in wt%) are indicated by the appearance of new peaks and the occurrence of some PS peak shifting in the PVK–PS polymer composites. The PS peaks at 1601, 1493, 1028, 756, and 698 cm^{-1}, which are attributed to C–H deformation and skeletal vibrations, shifted to 1599, 1491, 1026, 746, and 697 cm^{-1} in PVK-30, and to 1598, 1485, 1026, 746, and 696 cm^{-1} in PVK-50, respectively. Figure 2 shows the UV–Vis absorption spectra of PS, PVK, PVK-30, and PVK-50 polymer composites in solution. The UV–Vis absorption bands of them were summarized in Table 2. PS shows a strong band between 240 and 280 nm (262 nm maximum) [24, 25], which is attributed to the presence of a phenyl ring in each of its repeat unit. Similarly, PVK shows absorption bands at around 240, 262, 295, 320, and 340 nm, all of

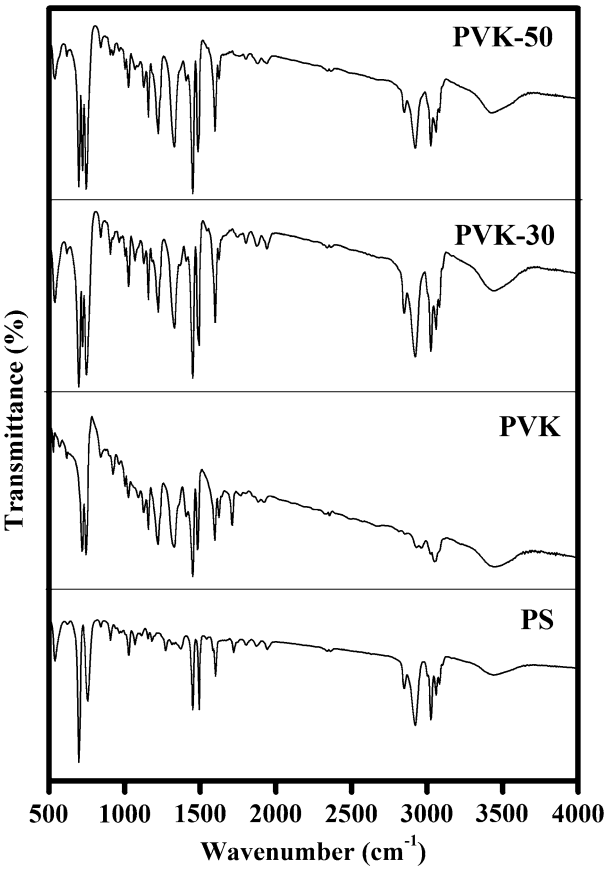

Fig. 1 FTIR spectra of PS, PVK, PVK-30, and PVK-50 polymer composites

Table 1 FTIR band assignments of the synthesized PS, PVK, PVK-30, and PVK-50

Assignments	Observed bands (cm^{-1})			
	PS	PVK	PVK-30	PVK-50
Ring deformation of substituted aromatic structure	698; 756	720; 744	697; 746	696; 746
C=C in aromatic ring	1,028		1,026	1,026
C–H in-plane deformation of aromatic ring		1,158		
C–N stretching of vinylcarbazole		1,221		
C–H deformation of vinylidene group		1,332		
$>CH_2$ deformation of vinylidene group		1,458		
Ring vibration of *N*-vinylcarbazole moiety		1,484		
C–H stretching of aromatic ring	1,493		1,491	1,485
C=C stretching vibration of vinylidene group	1,601	1,626	1,599	1,598
C–H stretching of –CH and $–CH_2$	2,920	2,926	2,919	2,917
C–H stretching of aromatic ring	3,025	3,048	3,023	3,021

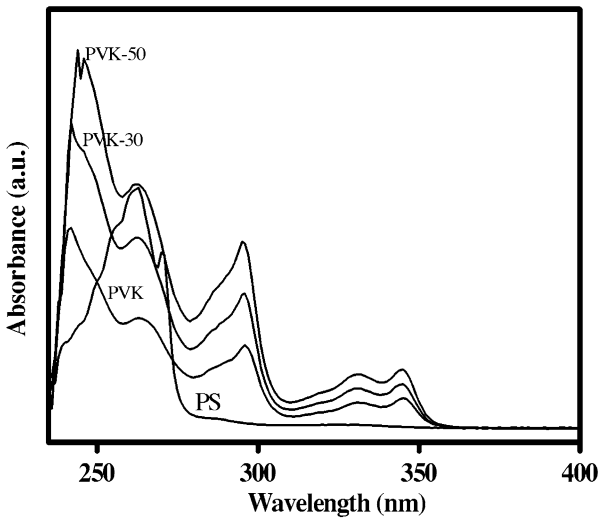

Fig. 2 UV–Vis spectra of PS, PVK, PVK-30, and PVK-50 polymer composites

Table 2 Summary of UV–Vis absorption bands observed for the synthesized PS, PVK, PVK-30, and PVK-50

Samples	Absortion bands (nm)				
PS	–	262	–	–	–
PVK	240	262	295	328	344
PVK-30	242	262	295	329	345
PVK-50	243	262	295	329	345

which are similar to the PVK peaks reported in literature [26]. The absorption band for PS in the PVK-30 and PVK-50 polymer composites appears to overlap with that of PVK. As can be observed in Fig. 2 and Table 2, other PVK peaks are red-shifted by 1–3 nm in the polymer composites, suggesting a possible conjugation between the PS and PVK polymers. The red-shift phenomenon may be attributed to the increased polymer chain interaction between the PVK and PS polymers.

Thermal behavior of PS, PVK, and PVK–PS composites

The TGA curves and DSC thermograms of PS, PVK, and PVK–PS composites are shown in Fig. 3a, b and respectively. Table 3 shows the comparative weight losses of PVK, PS, and the PVK–PS composites at different temperatures.

Figure 3a and Table 3 show that PVK exhibits approximately three to four stages of degradation. The first stage of degradation occurs in temperatures ranging from room temperature to 150 °C, which corresponds to moisture loss on the polymer surface. The second stage proceeds at temperatures between 150 and 320 °C and is attributed to the degradation of the primary chain of the phenyl ring. Weight losses

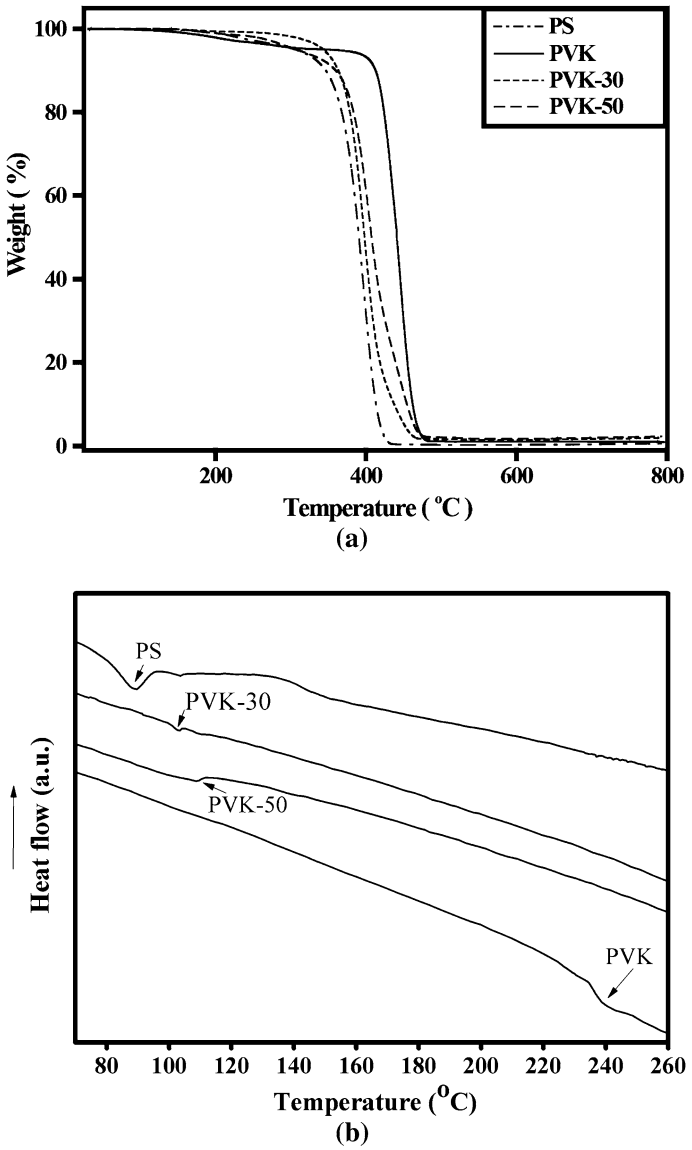

Fig. 3 TGA and DSC curves for PS, PVK, PVK-30, and PVK-50 polymer composites: **a** TGA curves. **b** DSC curves

after 320 °C, considered as the third stage of degradation, may be attributed to the complete degradation and decomposition of the polymer matrix [27]. For the PS homopolymer, the first stage of degradation occurs at temperatures ranging from room temperature to 150 °C, which corresponds to moisture loss on the polymer surface. Based on the TGA curves, the primary step of PS degradation is from 300 to 450 °C, which is attributed to the degradation of the main chain [28] and

Table 3 Weight losses of PVK, PS, and the PVK–PS composites at different temperatures

Samples	Weight loss (% wt) at different temperatures (°C)			
	200	400	600	800
PS	0.05	55.54	100	100
PVK	2.07	6.73	98.97	99.07
PVK-30	0.54	46.36	98.55	98.07
PVK-50	0.96	33.42	98.35	97.74

commences at around 340 °C with the evolution of aromatics from the degradation of styrene. Overall, the degradation patterns of the PVK and PS homopolymers, as well as that of the PVK-30 and PVK-50 polymer composites, are similar. The decrease in thermal stability of the PVK–PS composites is negligible compared with that of PVK, as can be observed in the PVK, PS, and PVK–PS thermograms (Fig. 3a). At 350–450 °C, the PVK–PS composites exhibit lower thermal stabilities than PVK, but higher thermal stabilities than PS. Below 350 °C and above 450 °C, the thermal behavior of the PVK and PS homopolymers, as well as those of the PVK–PS composites, remains more or less similar.

Figure 3b shows the glass transition temperature (T_g) of PS, PVK, and the PVK–PS composites, which indicates a pseudo second-order phase transition. The T_g of pure PVK is higher than that of PS and the PVK–PS composites. The T_g of pure PS was observed at 90 °C and shifted to 103 and 109 °C in the PVK-30 and PVK-50 composites, respectively. The incorporation of PVK into the PS matrix resulted in an increase in T_g. This effect may be due to motion restrictions of the polymer chains at the PVK/PS interface. A region of strongly bonded polymer chains might have formed in the PS matrix, where in the chains exhibit behaviors different from those observed in the homopolymer, and a strong packing force may hinders the mobility of the segmental chains. Therefore, more energy is needed to allow the first thermal transition, thereby shifting T_g to a higher temperature. In this case, similar effect might have occurred because of radical polymerization of NVK in the presence of PS. The observed increase in T_g with increasing PVK concentrations suggests good interfacial compatibility between PS and PVK.

Honeycomb-patterned structure of PVK and PVK–PS polymer composite films

Figure 4a–d shows typical SEM images of the PVK, PVK-15, PVK-30, and PVK-50 honeycomb-patterned films, respectively. The first two images show the surface structures, and the other images are cross-sectional views. The patterned PVK film shows an irregular structure (Fig. 4a). The differences between the diameters and pore heights of the large and small pores are significant. In addition, the film was very brittle, fragile, and unstable. Compared with the PVK film, the PVK–PS composite films show fairly regular structures in terms of both pore diameter and height. As shown in Fig. 4b, the PVK-15 film has a honeycomb pattern with circular pores. No significant difference between the pore diameter and pore height of its

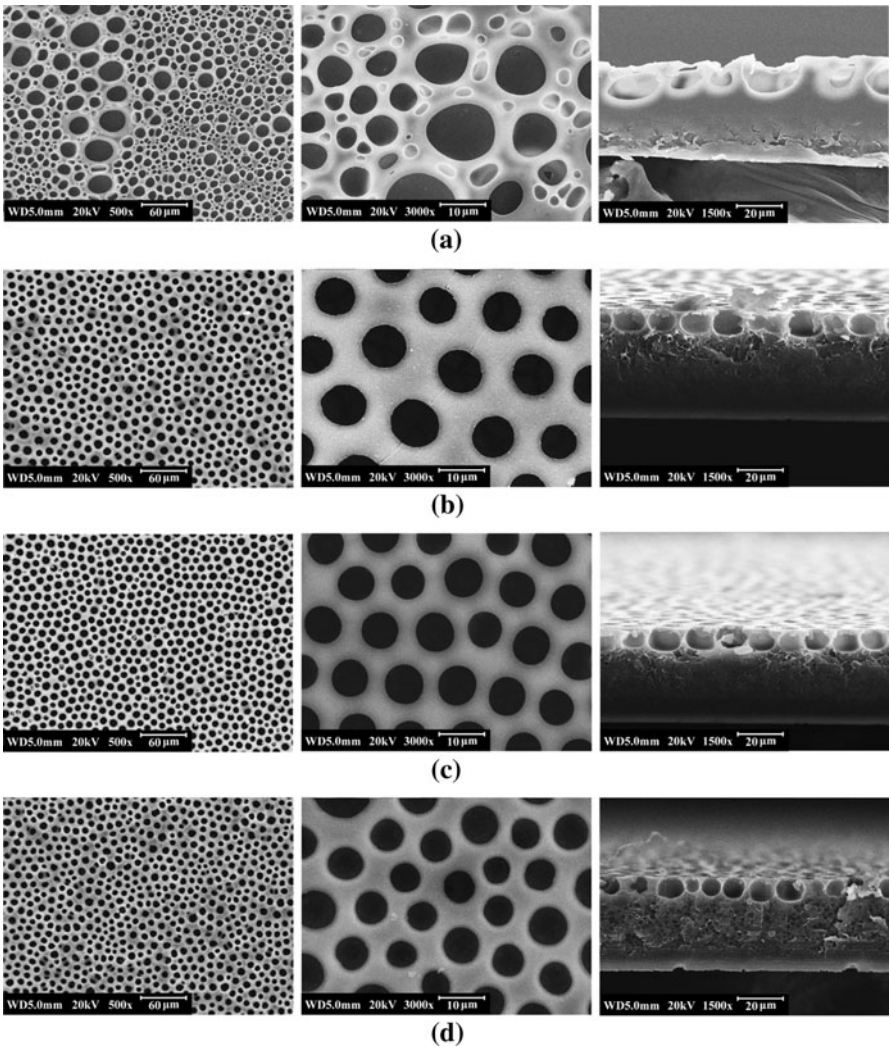

Fig. 4 SEM images: top-view (*left and center*) and cross-sectional view (*right*) of **a** PVK, **b** PVK-15, **c** PVK-30, and **d** PVK-50 films

large and small spherically ordered structures was observed. The approximate average diameter of these ordered structures was 10 μm. Similarly ordered structures were also observed in the PVK-30 film (Fig. 4c). However, its average pore diameter is slightly smaller than that of the PVK-15 film pores. A highly ordered honeycomb-patterned structure similar to that of the PVK-15 and PVK-30 films was observed in the PVK-50 film (Fig. 4d). However, the difference in the diameter of its large and small pores slightly increased. The approximate diameter of the larger pores was 8 μm, whereas that of the smaller pores was 5 μm. This difference may be attributed to the process that transformed the irregular pattern of

pure PVK film into the highly ordered pattern seen in the PVK–PS composites. The balancing of hydrophobicity through the interaction between PVK and PS in the composites resulted in more regular honeycomb patterns in the PVK–PS composites, compared with that of the pure PVK polymer. A similar phenomenon may explain the variation in the pore height of the composite films, which depends on PVK concentration. As shown in the cross-sectional images, the average pore heights for PVK-15, PVK-30, and PVK-50 were 10.5, 9.0, and 8.0 μm, respectively. In the porous films of PS and PVK, the pore diameter and pore height of PS are generally larger than those of PVK [29]. Given that the composites were synthesized using PS and different concentrations of PVK, the increasing PVK concentration in the composites justifies the decreasing pore dimensions observed in the PVK–PS honeycomb-patterned films. The SEM images of the patterned structure of the PVK, PVK-15, PVK-30, and PVK-50 films in Fig. 4 show the formation of the PVK–PS polymer composites.

Langmuir isotherm for the PVK–PS films

Figure 5 shows the surface pressure–area (Π–*A*) isotherm curves for the PVK-15, PVK-30, and PVK-50 films as a function of barrier speed at 2.5 mm s^{-1}. For reference, the curve for PVK is shown in the inset figure. The surface pressure increases with the increase in PVK concentration in the composites. The arrows indicate the forward and backward movements of the curves during the measurement. The surface pressure of the three ordered films appears expanded at lower barrier distances (10–30 mm). Further increase in pressure results in a condensed phase. In general, film stability is associated with a high-collapse pressure, a steep increase in the condensed phase, and a small hysteresis in the compression–expansion cycle. A steep increase in the condensed phase was also observed in the PVK-15, PVK-30, and PVK-50 polymer films. The average surface pressure for the PVK–PS films was within 65–70 mN m^{-1} at a barrier speed of 2.5 mm s^{-1}. Based on the isotherm analysis, the applied surface pressure on PVK-50 is relatively high compared with that on the PVK film. Thus, the addition of PS into the PVK polymer for the fabrication of the composites has a positive effect on the Π–*A* isotherms.

Photocurrent measurements

Figure 6 shows the photocurrent generation with the excitation by visible light ($\lambda > 500$ nm) in 10^{-2} mol dm^{-3} $LiClO_4$ at 0.4 V, for the PVK, PVK-15, PVK-30, and PVK-50 polymer composite films. The photocurrent generation responded to the on/off illumination cycles. The potential of the working electrode was set at 0.4 V (vs. Ag/AgCl). A nearly uniform photocurrent response was observed during each illumination cycle. As observed in Fig. 6a, the cathodic photocurrent response of the PVK film was 0.32×10^{-7} A cm^{-2}. Previous studies have also reported this range of photocurrent values for PVK in the Langmuir–Schaefer (LS) film [30–32]. Figure 6b shows that the photocurrent rise time for the PVK–PS films is shorter than the time between light switch-off and switch-on. The photocurrent values of the PVK-30 and PVK-50 films are higher compared to that of the PVK film.

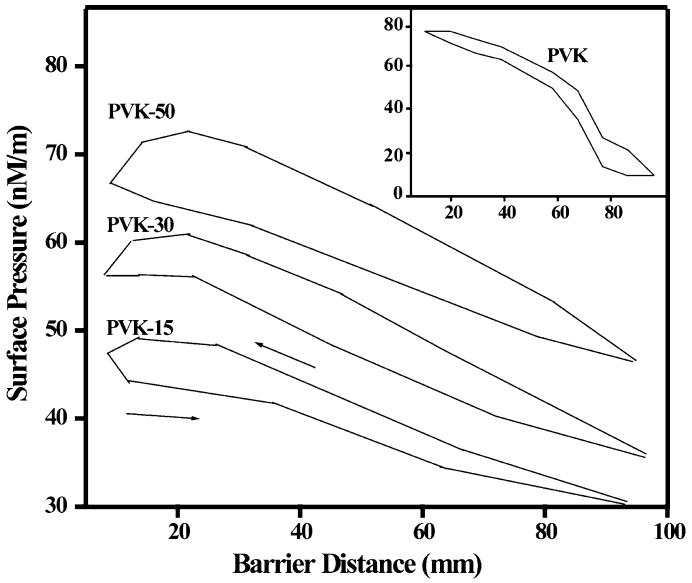

Fig. 5 Langmuir isotherm curves for the honeycomb-patterned PVK (*inset*), PVK-15, PVK-30, and PVK-50 films as a function of barrier speed (2.5 mm s^{-1})

The increases in the sample current under illumination for PVK-15, PVK-30, and PVK-50 were from 5 to 8 × 10^{-8} A cm^{-2}, 0.6 to 1 × 10^{-5} A cm^{-2}, and 5 to 7 × 10^{-5} A cm^{-2}, respectively. This increase can be attributed to differences in the film structures. In the porous films, the honeycomb structure plays an important role in enhancing the photocurrent generation. The porous structures significantly improve the light-capturing ability of the materials by enhancing light absorption [18]. The surface area of the porous film with the honeycomb pattern is larger than that of the smooth films. This larger surface area is responsible for the increased light absorption. Thus, compared with that of the flat surfaces, the photocurrent generation in the porous films is significantly higher.

The photocurrents observed in PVK-50 film are approximately 1,000 times higher than those observed in PVK and PVK-15 films. This difference may be attributed to the increase in the overall conductivity of the film, resulting in a more pronounced increase under illumination. The system shows a remarkable rectification behavior at the +0.4 V potential versus Ag/AgCl under visible light illumination. These observations indicate that the device efficiency of the PVK–PS patterned films is enhanced with the increase in the PVK concentrations.

The FTIR and UV–Vis spectra, thermal behavior, and surface morphology data reveal an interaction between PS and PVK, indicating that a chemical modification has occurred in the formation of the composites. Moreover, the incorporation/doping of PS also increases the processability of the PVK–PS composites. The thermal stability of the composites is better than that of the PS, as they have retained the stability of PVK.

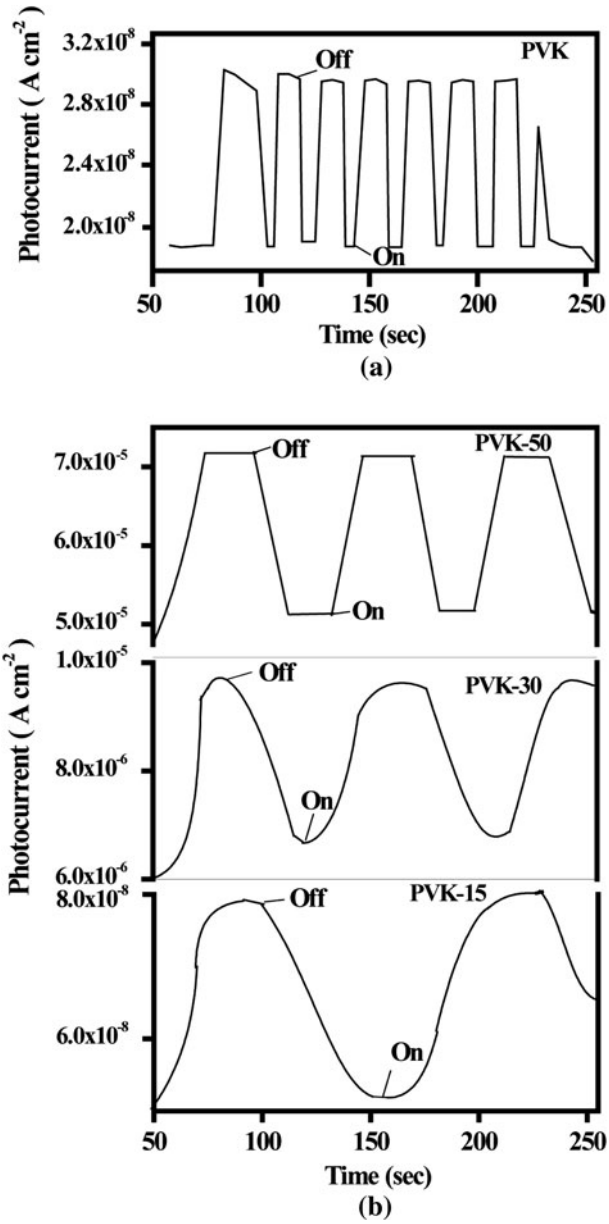

Fig. 6 Photo-chemical current measurements at 0.4 V in 10^{-2} mol dm^{-3} of $LiClO_4$ of **a** PVK film, **b** PVK-15, PVK-30, and PVK-50 films

Conclusion

New PVK–PS polymer composites with different PVK concentrations were synthesized via the polymerization of NVC in the presence of PS. The

incorporation/doping of PS into the PVK polymer increased the processability of the resulting PVK–PS composites. However, the thermal stability of the composites slightly decreased compared with that of the PVK homopolymer. The honeycomb-patterned films obtained from these composites under humid conditions had more regular and stable structures compared with those obtained from the PVK homopolymer alone. The photocurrent generation of the patterned films increased with the increase in the PVK concentration in the composites. The photocurrent values of the PVK-30 and PVK-50 films were higher than those of the PVK films. The methodologies employed in this study are simple and can be easily utilized for industrial applications. The PVK–PS composites and the films synthesized in this study can be used in the development of multi-component and -functional materials.

Acknowledgment This research was supported by the National Research Foundation of Korea (NRF) (2011-0025853).

References

1. Erdogan B, Song LL, Wilson JN, Park JO, Srinivasarao M, Bunz UHF (2004) Permanent bubble arrays from a cross-linked Poly(para-phenyleneethynylene): picoliter holes without microfabrication. J Am Chem Soc 126:3678–3679
2. Wan LS, Li JW, Ke BB, Xu ZK (2012) Ordered microporous membranes templated by breath figures for size-selective separation. J Am Chem Soc 134:95–98
3. Hedrick JL, Miller RD, Hawker CJ, Carter KR, Volksen W, Yoon DY, Trollsås M (1998) Templating nanoporosity in thin-film dielectric insulators. Adv Mater 10:1049–1053
4. Jiang P, Hwang KS, Mittleman DM, Bertone JF, Colvin VL (1999) Template-directed preparation of macroporous polymers with oriented and crystalline arrays of voids. J Am Chem Soc 121:11630–11637
5. Ostuni E, Chen CS, Ingber DE, Whitesides GM (2001) Selective deposition of proteins and cells in arrays of microwells. Langmuir 17:2828–2834
6. Yong TH, Lin CW, Cheng LP, Hsieh CC (2001) Preparation of EVAL membranes with smooth and particulate morphologies for neuronal culture. Biomaterials 22(13):1771–1777
7. Manz A, Becker H (eds) (1998) Microsystem technology in chemistry and life science. Springer, Berlin
8. Silverstein MS, Cameron NR, Hillmyer MA (2011) In: Porous polymers. Wiley-VCH, New Jersey
9. Wehrspohn RB (2005) Ordered porous nanostructures and applications. Springer, New York
10. Cai Y, Newby BZ (2009) Porous polymer films templated by marangoni flow-Induced water droplet arrays. Langmuir 25:7638–7645
11. Widawski G, Rawiso B, Francois B (1994) Self-organized honeycomb morphology of star-polymer polystyrene films. Nature 369:387–389
12. Pitois O, Francois B (1999) Formation of ordered micro-porous membranes. Eur Phys J B 8:225–231
13. Bunz UHF (2006) Breath figures as a dynamic templating method for polymers and nanomaterials. Adv Mater 18:973–989
14. Stenzel MH, Barner-Kowollik C, Davis TP (2006) Formation of honeycomb-structured, porous films via breath figures with different polymer architectures. J Polym Sci A 44:2363–2375
15. Malinauskas A, Malinauskiene J, Ramanavicius A (2005) Conducting polymer-based nanostructurized materials: electrochemical aspects. Nanotechnology 16:R51–R62
16. Pennwell RC, Gangully BN, Smith TW (1978) Poly(*N*-vinylcarbazole): a selective review of its polymerization, structure, properties, and electrical characteristics. J Polym Sci 13:63–160
17. D'Angelo P, Barra M, Cassinese A, Maglione MG, Vacca P, Minarini C, Rubino A (2007) Electrical transport properties characterization of PVK (poly *N*-vinylcarbazole) for electroluminescent devices applications. Solid-State Electron 51:123–129
18. Heng L, Zhai J, Zhao Y, Xu J, Sheng X, Jiang L (2006) Enhancement of photocurrent generation by honeycomb structures in organic thin films. ChemPhysChem 7:2520–2525

19. Ryttel A (1998) Copolymerization of styrene with *N*-vinylcarbazole in selected organic solvents. J Appl Polym Sci 67:715–721
20. Maul J, Frushour BG, Kontoff JR, Eichenauer H, Ott KH (2000) Polystyrene and styrene copolymers. In: Ullmann's Encyclopedia of Industrial Chemistry. Wiley-VCH, Weinheim
21. Yoon SJ, Chun H, Lee MS, Kim N (2009) Preparation of poly(*N*-vinylcarbazole) (PVK) nanoparticles by emulsion polymerization and PVK hollow particles. Synth Met 159:518–522
22. Kim BS, Basavaraja C, Jo EA, Kim DG, Huh DS (2010) Effect of amphiphilic copolymer containing ruthenium tris(bipyridyl) photosensitizer on the formation of honeycomb-patterned film. Polymer 51:3365–3371
23. Kaczmarek H, Felczak A, Szalla A (2008) Studies of photochemical transformations in polystyrene and styrenemaleic anhydride copolymer. Polym Degrad Stab 93:1259–1266
24. Zan L, Tian L, Liu Z, Peng Z (2004) A new polystyrene-TiO_2 nanocomposite film and its photocatalytic degradation. J Appl Catal A 264:237–242
25. Shang J, Chai M, Zhu Y (2003) Solid-phase photocatalytic degradation of polystyrene plastic with TiO_2 as photocatalyst. J Solid State Chem 174:104–110
26. Kang YO, Choi SH, Gopalan A, Lee KP, Kang HD, Song YS (2006) One-pot synthesis of a few nanocomposites with poly(*N*-vinylcarbazole) and CdS, Ag, Pd50-Ag50, and Pt50-Ru50 nanoparticles with γ irradiation. J Appl Polym Sci 100:1809–1815
27. Basavaraja C, Jo EA, Huh DS (2011) Fabrication and transport properties of poly(*N*-vinylcarbazole)-cellulose triacetate Langmuir–Schaefer films. Polym Compos 32:79–86
28. Suzuki M, Wilkie CA (2005) The thermal degradation of acrylonitrile–butadiene–styrene terpolymer as studied by TGA/FTIR. Polym Degrad Stab 47:217–221
29. Kim DG, Basavaraja C, Yamaguchi T, Huh DS (2012) Photo-controlled fabrication of self-organized structures in honeycomb-patterned thin films with light-sensitive amphiphilic copolymer. Polymer. doi:10.1016/j.polymer.2012.01.035
30. Basavaraja C, Kim WJ, Kim DG, Thin PX, Huh DS (2011) Enhanced surface morphology and transport property of poly(*N*-vinylcarbazole)/gold nanocomposite Langmuir–Schaefer films. Polym Compos 32:1077–1085
31. Bertoncello P, Notargiacomo A, Nicolini C (2004) Synthesis, fabrication and characterization of poly[3-3′(vinylcarbazole)] (PVK) Langmuir–Schaefer films. Polymer 45:1659–1664
32. Bertoncello P, Notargiacomo A, Erokhin V, Nicolini C (2006) Functionalization and photoelectrochemical characterization of poly[3-3′(vinylcarbazole)] multi-walled carbon nanotube (PVK-MWNT) Langmuir–Schaefer films. Nanotechnology 17:699–705